HEALTH AND MEDICINE

Nanovesicles derived from iron oxide nanoparticles–incorporated mesenchymal stem cells for cardiac repair

Ju-Ro Lee[1]*, Bong-Woo Park[2]*, Jonghoon Kim[1,3], Yeon Woong Choo[1], Han Young Kim[1], Jeong-Kee Yoon[1], Hyeok Kim[2,4], Ji-Won Hwang[2,4], Mikyung Kang[5], Sung Pil Kwon[1], Seuk Young Song[1], In Ok Ko[6], Ji-Ae Park[6], Kiwon Ban[7], Taeghwan Hyeon[1,3,8], Hun-Jun Park[2,4,9]†, Byung-Soo Kim[1,8]†

Because of poor engraftment and safety concerns regarding mesenchymal stem cell (MSC) therapy, MSC-derived exosomes have emerged as an alternative cell-free therapy for myocardial infarction (MI). However, the diffusion of exosomes out of the infarcted heart following injection and the low productivity limit the potential of clinical applications. Here, we developed exosome-mimetic extracellular nanovesicles (NVs) derived from iron oxide nanoparticles (IONPs)–incorporated MSCs (IONP-MSCs). The retention of injected IONP-MSC–derived NVs (IONP-NVs) within the infarcted heart was markedly augmented by magnetic guidance. Furthermore, IONPs significantly increased the levels of therapeutic molecules in IONP-MSCs and IONP-NVs, which can reduce the concern of low exosome productivity. The injection of IONP-NVs into the infarcted heart and magnetic guidance induced an early shift from the inflammation phase to the reparative phase, reduced apoptosis and fibrosis, and enhanced angiogenesis and cardiac function recovery. This approach can enhance the therapeutic potency of an MSC-derived NV therapy.

INTRODUCTION

Cardiovascular diseases including myocardial infarction (MI) and their related complications are major causes of death (*1*, *2*). MI is characterized by the restriction of blood flow in the infarction area and the subsequent death of cardiac cells. The implantation of mesenchymal stem cells (MSCs) can reduce the infarct size, prevent excessive tissue loss, and enhance cardiac function in animal MI models (*3*, *4*). However, the low survival of implanted MSCs limits their therapeutic potency (*5*, *6*). In addition, MSC implantation may cause arrhythmias or the differentiation of the MSCs into other types of cells including chondrocytes and osteocytes in the infarcted myocardium, or it may trigger tumorigenesis (*7*, *8*).

It has been revealed that implanted MSCs mediate cardiac repair mainly by secreting paracrine molecules rather than differentiating into cardiac cell lineages (*9*). Recent studies have shown that the therapeutic potential of MSCs is largely attributed to exosomes, which are a specific type of extracellular vesicles (EVs) that have diameters of 50 to 200 nm, contain RNAs and proteins, and are involved in intercellular communications by acting as carriers of bioactive molecules (*10*). Because of the enrichment of cardiac repair–favorable molecules in MSC-derived exosomes, they exert a cardiac

repair efficacy that is similar to that of implanted MSCs (*11*, *12*). RNAs and proteins in the exosomes transferred from the parental cells to the recipient cells are functional in the recipient cells and participate in the regulation of intracellular signaling cascades (*13*, *14*). In addition, MSC-derived exosomes can avoid the low cell survival issue, arrhythmia and tumorigenesis risk, and the immune response triggered by the MSC implantation therapy. They can also be stored at −80°C for a long period. Because of the safety concerns of MSC implantation and the advantages of using exosomes, the administration of MSC-derived exosomes has emerged as an alternative cell-free therapy for cardiac repair (*15*).

Despite the therapeutic potential of exosomes, their use in the clinical applications is not easily feasible because MSCs secrete exosomes in very small quantities. The average exosome yield from 10^6 cells is 1 to 4 μg/day (*16*), which cannot easily meet the quantity (100 to 500 μg per patient) of exosomes required in a clinical trial (*17*). Recently, exosome-mimetic nanovesicles (NVs), which have similar size and composition to those of exosomes, have been developed through the serial extrusion of cells through microporous filters (*18*, *19*). Similar to exosomes, NVs can also convey the biomolecules of their parental cells to recipient cells. NVs have advantages over exosomes, such as a 250-fold higher production yield and a 2-fold greater quantity of RNAs and proteins (*20*). Therefore, in this study, we applied MSC-derived NVs rather than MSC-derived exosomes in terms of clinical scale production, cost effectiveness, and therapeutic potency.

A number of studies have showed that, immediately after cell injection into the infarcted heart, most of the cells diffuse out from the injection area, which would limit their therapeutic potential. Here, we found that magnetic guidance of iron oxide nanoparticle (IONP)–incorporated NVs following injection could improve the retention of NVs in the infarcted heart. IONP is slowly ionized and assimilated in vivo (*21*), and the U.S. Food and Drug Administration has approved the clinical usage of IONP (ferumoxytol). In addition to the enhanced retention, we also found that NVs derived from IONP-incorporated MSCs (IONP-NVs) contained much larger

[1]School of Chemical and Biological Engineering, Seoul National University, Seoul 08826, Republic of Korea. [2]Department of Medical Life Science, College of Medicine, The Catholic University of Korea, Seoul 06591, Republic of Korea. [3]Center for Nanoparticle Research, Institute of Basic Science (IBS), Seoul 08826, Republic of Korea. [4]Division of Cardiology, Department of Internal Medicine, Seoul St. Mary's Hospital, Seoul 06591, Republic of Korea. [5]Interdisciplinary Program for Bioengineering, Seoul National University, Seoul 08826, Republic of Korea. [6]Division of Applied RI, Korea Institute Radiological and Medical Sciences, Seoul 01812, Republic of Korea. [7]Department of Biomedical Sciences, City University of Hong Kong, Kowloon Tong, Hong Kong. [8]Institute of Chemical Processes, Institute of Engineering Research, BIOMAX, Seoul National University, Seoul 08826, Republic of Korea. [9]Cell Death Disease Research Center, College of Medicine, The Catholic University of Korea, Seoul 06591, Republic of Korea.
*These authors contributed equally to this work.
†Corresponding author. Email: byungskim@snu.ac.kr (B.-S.K.); cardioman@catholic.ac.kr (H.-J.P.)

quantities of therapeutic molecules for cardiac repair (RNAs and proteins) than normal MSC–derived NVs (N-NVs), which are mediated by intracellular signaling modifications triggered by the ionization of IONPs in IONP-incorporated MSCs (IONP-MSCs) (fig. S1) (22–27). IONPs not only induced the up-regulation of hypoxia-inducible factor 1α (HIF1α)–mediated growth factor expression in MSCs, which is similar to hypoxia-induced (27) and heat shock–induced (28) up-regulation of HIF1α-mediated growth factor expression in MSCs, but also augmented the retention of NVs in the heart.

Therefore, we hypothesized that IONP-NVs would have stronger therapeutic potential for cardiac repair compared to those of N-NVs through enhanced retention by magnetic guidance and increased quantities of therapeutic molecules in IONP-NVs. We found that, similar to MSCs, IONP-NVs exhibited antiapoptotic, antifibrotic, anti-inflammatory, and proangiogenic effects on cardiac fibroblasts (CFs), cardiomyocytes (CMs), endothelial cells (ECs), and macrophages, which are the major therapeutic mechanisms of MSCs for cardiac repair in vitro. Following the injection of IONP-NVs, the retention of IONP-NVs in the infarcted myocardium was greatly enhanced by the application of a magnetic field for 24 hours. As a result, the IONP-NV injection resulted in reduced apoptosis, inflammation, and infarct size, as well as improved angiogenesis and cardiac function recovery. Overall, our data suggest that IONP-NVs may represent a highly effective and feasible cell-free therapy for MI.

RESULTS
Cellular uptake of IONPs triggers cellular modification of MSCs
We evaluated the physical and biological characteristics of IONPs. A transmission electron microscopy (TEM) image shows that IONPs were 20 to 30 nm in size and had a cubic shape (Fig. 1A). In the fluorescent microscope images obtained 24 hours after rhodamine B isothiocyanate (RITC) fluorescent dye–labeled IONP treatment to MSCs, IONPs were well internalized into the cytoplasm of MSCs (Fig. 1B). TEM images also showed that the internalized IONPs were retained within intracellular endosomes (fig. S2A). Quantitative evaluation revealed an iron content of 47 pg within one cell (fig. S2B). IONPs did not exhibit cytotoxic effects on MSCs, as evaluated with cholecystokinin (CCK) assay 2, 4, 7, 10, and 14 days after IONP treatment (Fig. 1C). Quantitative real-time reverse transcription polymerase chain reaction (qRT-PCR) analyses for apoptosis-related genes and the staining for fluorescein diacetate (FDA)/ethidium bromide (EB) 2 days after IONP treatment also showed no cytotoxic effects on the viability of MSCs (fig. S2, C and D). However, the treatment with the same molar concentration of iron ions ($Fe^{2+/3+}$) to MSCs exhibited a significant cytotoxicity compared to IONPs (fig. S2E). In addition, the IONP treatment stimulated the osteogenic and adipogenic differentiation of MSCs by up-regulation of some genes (*ALP*, *LPL*, and *PPARγ*) but not chondrogenic differentiation (fig. S2F). This result was different from that of a previous study in which IONP loading in MSCs did not stimulate osteogenic and adipogenic differentiation and inhibited chondrogenic differentiation (29). The inconsistency between two studies could be due to the difference in the IONP dose (47 pg of IONPs per cell in the present study versus 10 to 20 pg of IONPs per cell in the previous study).

We determined whether IONPs internalized in MSCs could affect gene expression levels of cardiac repair–related molecules in the MSCs. The IONP uptake significantly increased the expression

mRNA and protein levels of cardiac repair–favorable genes including angiopoietin-1 (ANG1), fibroblast growth factor 2 (FGF2), hepatocyte growth factor (HGF), vascular endothelial growth factor (VEGF), placental growth factor (PGF), and HIF1α, 2 days after IONP treatment, as evaluated with qRT-PCR and Western blot (Fig. 1, D and E). After cellular uptake, IONPs in the endosomes at a low pH may undergo slow ionization, releasing iron ions into the cytoplasm and generating reactive oxygen species (ROS) (22, 30, 31). The up-regulated expression levels of the cardiac repair–favorable genes may be due to the overproduction of ROS that not only activate c-Jun N-terminal kinase (JNK) (23) and c-Jun (24) but also up-regulate the expression of HIF1α (26, 27). Western blot analysis showed the up-regulated expression of HIF1α and activation of JNK and c-Jun 2 days after IONP treatment (Fig. 1E).

IONP-NVs derived from IONP-MSCs contain increased therapeutic molecules
We have prepared N-NVs and IONP-NVs by serial extrusion of MSCs and IONP-MSCs. The process of IONP-NV preparation and the portion of protein and IONPs of each fraction are shown in fig. S3A. We characterized N-NVs and IONP-NVs. TEM images and dynamic light scattering (DLS) analysis revealed that N-NVs and IONP-NVs had spherical shapes and their sizes were similar to the typical size of EVs [Fig. 2, A (i) and B] (32). TEM and fluorescent confocal images revealed that IONPs were entrapped inside IONP-NVs (Fig. 2A). Scanning TEM (STEM) and energy-dispersive x-ray spectroscopy (EDX) mapping images also indicate that IONPs were entrapped in IONP-NVs (fig. S3B). Inductively coupled plasma–mass spectrometry (ICP-MS) analysis showed an iron content of 21 ng within 1 μg of IONP-NVs (fig. S3C). To compare the quantities of proteins and RNAs of NVs with those of exosomes, we quantified the amounts of proteins and RNAs in IONP-MSC–derived exosomes and IONP-NVs (fig. S3D). IONP-NVs contain 2.0- to 2.5-fold larger quantities of proteins and RNAs than IONP-MSC–derived exosomes.

To compare the mRNA expression and protein levels in N-NVs and IONP-NVs, we performed qRT-PCR and Western blot. The data showed that the mRNA expression and protein levels of ANG1, FGF2, VEGF, PGF, HGF, connexin 43 (Cx43), and HIF1α were significantly higher in IONP-NVs compared to N-NVs (Fig. 2, C and D). Both N-NVs and IONP-NVs contained CD9, a marker for exosome, EV, and NV (19). The levels of cardiac repair–related microRNAs (miRNAs) were compared between N-NVs and IONP-NVs using Affymetrix miRNA 4.0 (Fig. 2E). Many miRNAs known to promote cardiac recovery were increased in IONP-NVs versus N-NVs. In addition, we analyzed changes in gene expressions between N-NVs and IONP-NVs using RNA sequencing (fig. S3, E to G). Expressions of a total 227 genes were significantly changed in IONP-NVs versus N-NVs.

To evaluate NV uptake by individual cell levels in cardiac tissue, we performed fluorescent microscopic examination 24 hours after the treatment of CFs, CMs, human umbilical vein ECs (HUVECs), and macrophages with N-NVs and IONP-NVs in vitro (fig. S4A). As shown in fig. S4B, most of the treated IONP-NVs were internalized into the cells in vitro within 24 hours after treatment. To evaluate the cytotoxicity of IONPs inside the cells, we assessed the viability of CFs, CMs, HUVECs, and macrophages 2, 5, and 10 days after treatment with IONP or IONP-NV (fig. S4C). IONPs did not affect the cellular viability for a long term. After internalization, the IONPs were slowly ionized and degraded, as the iron content in the cells decreased with time (fig. S4D) and as reported previously (33).
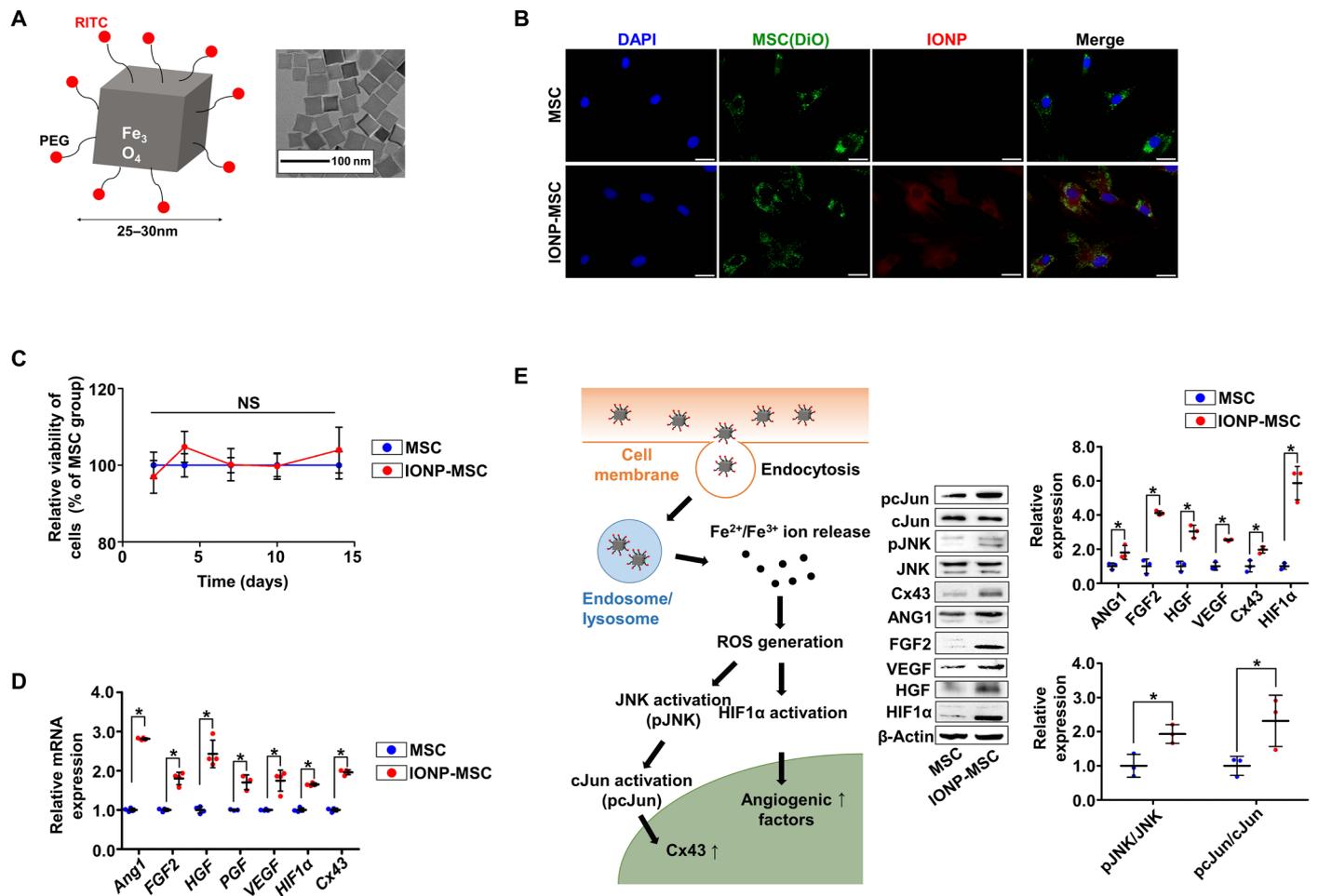
Fig. 1. Cellular uptake of IONPs and IONP-triggered cellular modification. (**A**) Schematic illustration and TEM image of IONPs. PEG, polyethylene glycol. (**B**) Fluorescent images of IONP (red) uptake by MSCs 24 hours after IONP treatment [green, cell membrane; and blue, 4′,6-diamidino-2-phenylindole (DAPI)]. Scale bars, 100 μm. (**C**) The cytotoxicity of IONPs 2, 4, 7, 10, and 14 days after IONP treatment to MSCs, as evaluated by CCK assay (*n* = 4 per group; NS, no significant difference). (**D**) Relative mRNA expression levels of various cardiac repair–favorable genes in MSC and IONP-MSC, as evaluated by qRT-PCR (*n* = 4 per group). (**E**) Schematic illustration of the IONP-mediated intracellular signaling cascades in MSCs and Western blot analysis for the intracellular signaling cascade molecules and associated therapeutic molecules (*n* = 3 per group). **P* < 0.05 by two-tailed *t* test. All values are means ± SD.

Therapeutic effects of IONP-NVs in vitro

To assess the therapeutic effects of IONP-NV, we used CMs, CFs, HUVECs, and macrophages in vitro. To determine whether IONP-NVs have the therapeutic potential for cardiac repair, we assessed the antiapoptotic and antifibrotic effects of NVs and MSCs on CFs, CMs, and HUVECs in vitro. The cells were cocultured with MSCs or IONP-MSCs or treated with IONPs, N-NVs, or IONP-NVs for 1 day after exposure to a hypoxic condition that mimicked cardiac ischemia (fig. S5A). In the IONP alone group, the quantity of IONPs was equal to that of IONP-NVs (21 ng of iron in IONPs/1 μg of NV protein). Both NVs and MSCs showed the cardioprotective effect on the cells after hypoxia (Fig. 3A). Gene expression of caspase-3 and FDA/EB staining data also showed that NVs and MSCs improved the cell viability and attenuated apoptosis of the cells (fig. S5, B and C). Western blot analysis showed that both IONP-NVs and IONP-MSCs exerted the cardioprotective effect via activating AKT/ phosphatidylinositol 3-kinase (PI3K) (*34*) intracellular signaling cascades (fig. S5, D and E).

The mRNA expression of Cx43 was up-regulated in CFs and CMs under hypoxic condition by NVs and MSCs (fig. S5F). In addition, Western blots and immunocytochemistry showed that Cx43 expression in CFs and CMs was up-regulated by IONP-NVs and IONP-MSCs (fig. S5, G and H). Cx43 is well known to have functions as electrical coupling and intercellular molecule exchange of CFs and CMs. There were several reports that Cx43 expression was decreased in hypoxic condition, which causes arrhythmia and cardiac cell death due to decreased conduction between cells in vitro and in vivo (*35*, *36*).

To investigate the antifibrotic effects of NVs and MSCs, we evaluated gene expression changes in CFs using qRT-PCR (Fig. 3B). NVs and MSCs decreased the expression of the transforming growth factor β1 (*Tgfb1*), α-actin 2 (*Acta2*), and matrix metalloproteinases (*Mmp2* and *Mmp9*) and increased the tissue inhibitors of metalloproteinases (*Timp1* and *Timp2*), which are the marker of cardiac myofibroblast, within CFs. The data indicate that NVs and MSCs inhibited the differentiation of CFs into cardiac myofibroblasts after hypoxia, which
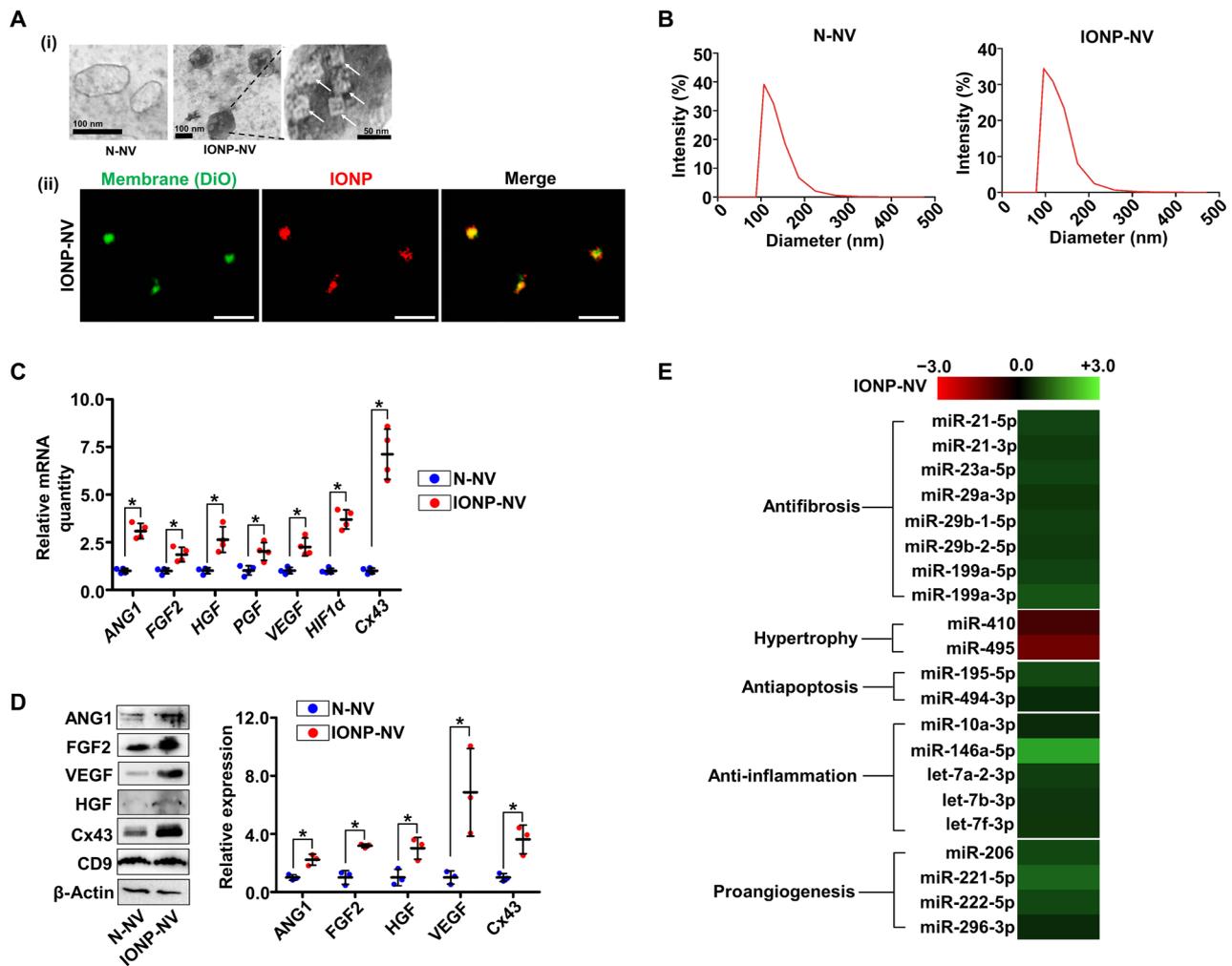
Fig. 2. Preparation and characterization of MSC-derived NVs. (A) (i) TEM images of N-NVs and IONP-NVs and (ii) confocal images of IONP-NVs. White arrows indicate IONPs within IONP-NVs. In the fluorescent confocal images, NV lipid layers and IONPs were labeled with DiO (green) and RITC (red), respectively. Scale bars, 1 μm (ii). **(B)** Representative size distribution of N-NVs and IONP-NVs derived from MSCs and IONP-MSCs, respectively, as evaluated by DLS. **(C)** Relative mRNA levels in N-NVs and IONP-NVs, as evaluated by qRT-PCR ($n = 4$ per group). **(D)** Representative images of Western blots of therapeutic molecules and the marker of EV, CD9 ($n = 3$ per group). **(E)** Fold changes in levels of cardiac repair–related microRNA (miRNA) in IONP-NVs compared to N-NVs. All columns represent $\log_2$-fold changes. *$P < 0.05$ by two-tailed t test. All values are means ± SD.

are the major cause of cardiac fibrosis and remodeling. Both IONP-NVs and IONP-MSCs exerted higher antifibrotic effects than those of N-NVs and MSCs, respectively. Together, these results demonstrate that IONP-NVs can attenuate cell death and prevent fibrosis, as MSCs do.

We next examined the anti-inflammatory effects of NVs and MSCs on cells, including CFs, CMs, and macrophages in vitro. The experimental protocol is described in fig. S5A. We examined the effects of NVs and MSCs on the phenotype change in M1 macrophages. NVs and MSCs down-regulated the mRNA expression levels of inflammatory M1 macrophage markers and up-regulated those of reparative M2 macrophage markers (Fig. 3C). M0 macrophages served as a control. IONP-NVs and IONP-MSCs exerted stronger effects on the M1 macrophage shift to M2 macrophage than N-NVs and MSCs, respectively. In addition, NVs and MSCs decreased the mRNA expression levels of proinflammatory cytokines including *Il6* and *Tnfa* in CFs and CMs (fig. S5I). IONP-NVs and IONP-MSCs exerted a higher anti-inflammatory effect on CFs and CMs than

N-NVs and MSCs, respectively. Thus, our data indicate that, similar to MSC implantation, IONP-NV treatment can exert anti-inflammatory effects via polarizing M1 macrophages into M2 phenotype and reducing inflammatory cytokine production of CMs and CFs.

We further evaluated the proangiogenic effects of NVs and MSCs in vitro. NVs and MSCs stimulated the capillary formation of HUVECs cultured under hypoxic conditions (Fig. 3, D and E). IONP-NVs exerted a higher effect on tube formation compared to N-NVs. The enhanced capillary formation may be mediated via activating extracellular signal–regulated kinase (ERK) and proliferating cell nuclear antigen (PCNA) signaling in HUVECs (fig. S5J), which inhibits p38 that is known to break down capillary tubes (*37*). In addition, proliferating HUVECs also increased, which may result in increased capillary tube formation. HUVEC migration was reduced by hypoxia and returned back to normal by NVs and MSCs. IONP-NVs and IONP-MSCs exerted higher effects on the HUVEC migration than N-NVs and MSCs, respectively.
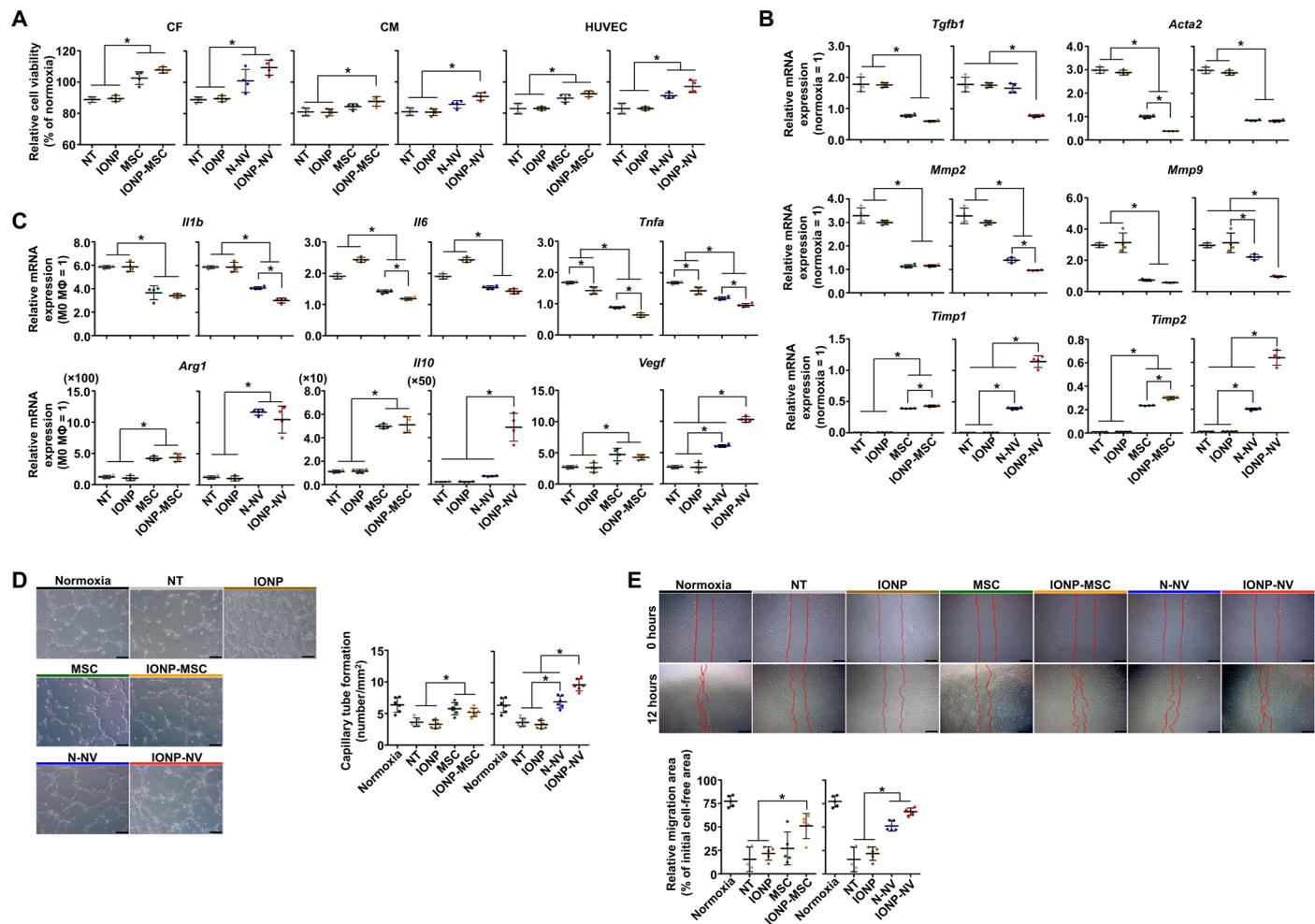
Fig. 3. Therapeutic effects of IONP-NVs in vitro. (**A**) Relative cell viability as evaluated by the CCK assay after treatment (*n* = 4 per group). (**B**) Antifibrotic effects of NVs and MSCs. Relative mRNA expression levels of cardiac myofibroblast–related genes in CFs after treatment, as evaluated by qRT-PCR (*n* = 4 per group). (**C**) Macrophage (MΦ) polarization after treatment. Relative mRNA expression levels of the markers of inflammatory M1 macrophages (*Il1b*, *Il6*, and *Tnfa*) and reparative M2 macrophages (*Arg1*, *Il10*, and *Vegf*) in lipopolysaccharide (LPS)–treated macrophages (M1 MΦ) after treatment, as evaluated by qRT-PCR (*n* = 4 per group). All data were normalized to normoxia or M0 MΦ data. (**D** and **E**) Capillary tube formation (*n* = 6 per group) and cell migration (*n* = 5 per group) of HUVECs after treatment. Red lines indicate borders of the cell-free area. Scale bars, 200 and 500 μm, respectively. NT indicates no treatment. *$P < 0.05$, using one-way analysis of variance (ANOVA), followed by post hoc Bonferroni test. All values are means ± SD.

Synthetically, we demonstrated that, similar to MSCs, IONP-NVs exhibit therapeutic effects on CFs, CMs, HUVECs, and macrophages in vitro. IONP-NVs not only reduced apoptosis, fibrosis, and inflammation but also increased angiogenesis, which is the major mechanism of MSCs for cardiac repair. Thus, the data suggest that IONP-NVs can be an effective cell-free option that replaces MSC implantation therapy for cardiac repair.

Magnetic guidance increases the retention of IONP-NVs in the infarcted myocardium

To determine whether NVs are superior to MSCs for retention in the myocardium and whether magnetic guidance enhances the retention of IONP-NVs in the myocardium, we intramyocardially injected MSCs, IONP-MSCs, N-NVs, and IONP-NVs, both of which were labeled with fluorescent dyes, and magnetic guidance was applied for 24 hours. The data showed that NVs were superior to MSCs for retention in the myocardium 24 hours after injection

(Fig. 4A). Furthermore, IONP-NV + M (magnetic guidance) group exhibited the highest retention in the heart. The biodistribution of the MSCs and NVs in other organs of the animals is shown in fig. S6A. In addition, the retention ratio of IONP-NVs with magnetic guidance was gradually decreased in the infarcted heart with the time (fig. S6B). To compare the therapeutic efficacy of MSCs and IONP-NVs, we assessed the therapeutic growth factor expression in the heart and cardiac function after the implantation of MSCs and the injection of IONP-NVs. The data showed that the expression of growth factors including VEGF and HGF was significantly lower in the MSC implantation group as compared to the IONP-NV + M group (fig. S6C). This is likely attributed to the low survival of MSCs implanted to hypoxic and inflammatory infarction area of the heart (*38*). As a result, cardiac function was significantly higher in the IONP-NV + M group as compared to the MSC group (fig. S6, D to F). Because of the larger therapeutic effects of NVs than MSCs, we used NVs rather than MSCs in the following animal experiments. To further
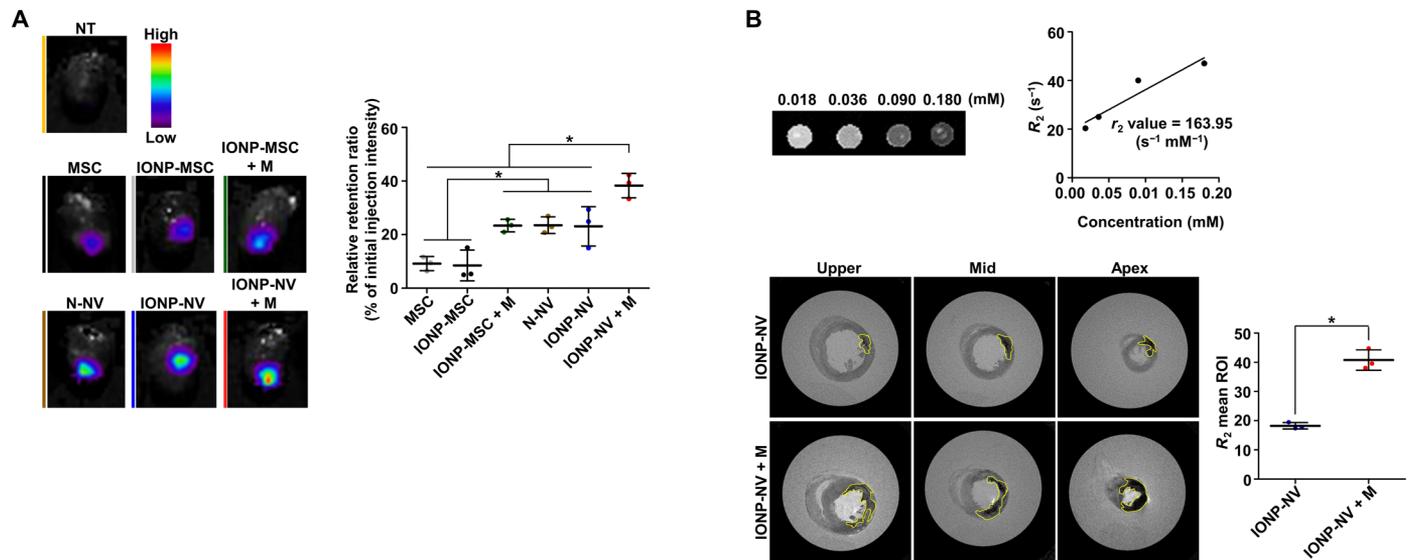
Fig. 4. Retention of IONP-NVs in the infarcted myocardium. Fluorescent dye–labeled IONP-MSCs and IONP-NVs were injected into the rat infarcted myocardium. In some groups, magnetic guidance (M) was applied above the hearts for 24 hours after injection. (**A**) Representative ex vivo fluorescent imaging of infarcted hearts and the quantitative data 24 hours after the injection of VivoTrack 680–labeled MSCs, IONP-MSCs, N-NVs, and IONP-NVs ($n = 3$ animals per group). VivoTrack 680 labeled the membranes of cells and NVs. *$P < 0.05$, using one-way ANOVA, followed by post hoc Bonferroni test. (**B**) Representative magnetic resonance images and the quantification of IONP within heart 24 hours after the injection of IONP-NVs ($n = 3$ animals per group). The yellow line indicates IONP retention area. *$P < 0.05$, using two-tailed t test. All values are means ± SD. ROI, region of interest.

assess the increased retention of IONP-NVs by magnetic guidance, we used magnetic resonance imaging (MRI) analysis, as previously described (*39*). As shown in Fig. 4B, r_2 (transverse relaxation rate per 1 mM iron) value of IONP was 163.95 s^{-1} mM^{-1}, and the retention of IONP-NVs was significantly augmented by magnetic guidance. Fluorescent images and the quantification data also indicate that IONP-NVs with magnetic guidance exhibited the highest retention in the infarcted myocardium (fig. S6G). To determine whether IONPs with magnetic guidance exhibit cytotoxic effects in vivo, we performed terminal deoxynucleotidyl transferase–mediated deoxyuridine triphosphate nick end labeling (TUNEL) assay 24 hours after IONP-NVs injection into the normal hearts (fig. S7A). Magnetic field–applied IONPs did not exhibit the cytotoxic effect on cells in vivo. In addition, the levels of hepatic enzymes [aspartate aminotransferase (AST) and alanine aminotransferase (ALT)], blood urea nitrogen (BUN), and creatinine were not significantly different from those of the normal group 1, 3, 7, 14, 21, and 28 days after injection (fig. S7B). Furthermore, to determine whether IONPs remain in the heart or travel to other organs, we stained IONPs using Prussian blue staining in major organs 1 and 4 weeks after injection (fig. S8). IONPs were not detected in organs except in the heart. In addition, IONPs were decreased in the heart with time.

IONP-NVs with magnetic guidance attenuate cell apoptosis and inflammation in vivo
To investigate the antiapoptotic effects of IONP-NVs in the infarcted myocardium, we performed the TUNEL assay 24 hours after injection (Fig. 5A). In the border zone, cell apoptosis was reduced by the injection of either N-NVs or IONP-NVs and further decreased in the IONP-NV + M group. In the infarct zone, only the IONP-NV + M group exhibited decreased apoptosis. The Cx43 expression in the peri-infarct zone was assessed with immunohistochemistry (Fig. 5B). The IONP-NV + M group exhibited a higher level of Cx43 in the

peri-infarct zone compared to the other groups, which may be attributed to the reduction of cell death and arrhythmia at the early stage of infarction.

Next, we examined the anti-inflammatory effects of NVs in the infarcted myocardium through evaluation of macrophage polarization 1 day after injection (Fig. 5C). The data showed that only the IONP-NV + M group exhibited up-regulated expression levels of reparative M2 macrophage–specific markers (*Cd206*, *Arg1*, and *Il10*). The N-NV, IONP-NV, and IONP-NV + M groups down-regulated expression levels of M1 macrophage–specific markers (*Nos2*, *Il1b*, and *Il6*). Immunohistochemistry showed that the IONP-NV + M group significantly up-regulated CD206 expression and down-regulated nitric oxide synthase (NOS2) expression in CD68-positive macrophages in the peri-infarct zone (Fig. 5D). The data suggest that IONP-NVs can effectively induce early transition of the inflammatory phase to the reparative phase by facilitating the rapid polarization of M1 macrophages into M2 macrophages, which may elicit cardiac repair after MI, as a previous study revealed (*40*).

IONP-NVs increase blood vessel density, improve left ventricular remodeling, and promote cardiac function recovery
To determine whether the NV injection into the infarcted myocardium enhances the blood vessel density, we perfused hearts with isolectin B4 4 weeks after MI (Fig. 6A). The IONP-NV + M group exhibited a significant increase in the blood vessel density in both the border zone and infarct zone, compared to the other groups. In addition, IONP-NV also increased the blood vessel density in the border zone and infarct zone as compared to the no treatment (NT) group. This may be attributed to the attenuation of early apoptosis of the ECs (Figs. 3A and 5A) and the stimulation of migration, proliferation, and tube formation of the ECs (Fig. 3, D and E).
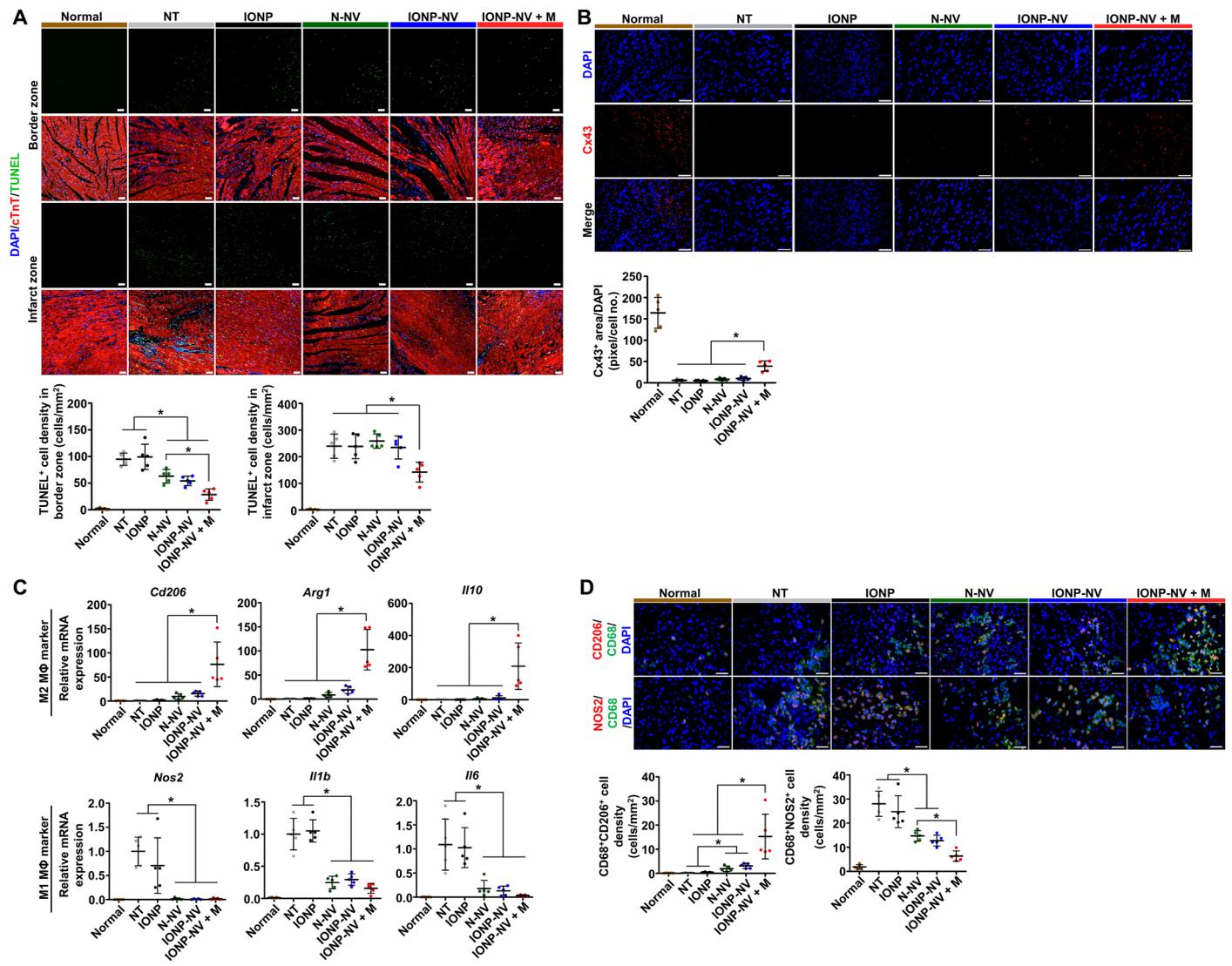
Fig. 5. Attenuation of cell apoptosis and inflammation by IONP-NV injection in vivo. (**A**) Representative images of TUNEL-positive (green) apoptotic cells and immuno-staining for cardiac troponin T (cTnT) (CM marker) and the quantitative data 1 day after injection (*n* = 5 animals per group). Scale bars, 100 μm. (**B**) Representative images of immunohistochemical staining for Cx43 in the peri-infarct zone and the quantitative data 1 day after injection (*n* = 5 animals per group). Scale bars, 100 μm. (**C**) Relative mRNA expression levels of M2 macrophage–specific markers (*Cd206*, *Arg1*, and *Il10*) and M1 macrophage–specific markers (*Nos2*, *Il1b*, and *Il6*) in the infarcted myocardium, as evaluated by qRT-PCR (*n* = 5 animals per group). (**D**) Immunohistochemical staining for CD68 (macrophage marker), CD206 (M2 macrophage marker), and nitric oxide synthase 2 (NOS2) (M1 macrophage marker); and the quantitative data in the peri-infarct zone 1 day after injection (*n* = 5 animals per group). Scale bars, 50 μm. *$P < 0.05$, using one-way ANOVA, followed by post hoc Bonferroni test. All values are means ± SD.

Four weeks after treatment, the multiple sections of heart tissue were stained with Masson's trichrome staining (Fig. 6B and fig. S9). The IONP-NV injection and magnetic guidance resulted in a significant decrease in the fibrosis area and scar size and increase in the viable myocardium area and infarcted wall thickness in the infarcted heart (Fig. 6C). In addition, IONP-NV also decreased fibrosis area and increased infarcted wall thickness as compared to the NT group and the IONP group.

To evaluate cardiac functional recovery, we performed transthoracic echocardiography 1, 2, and 4 weeks after MI (Fig. 6, D to F). All groups except the IONP-NV + M group showed a significant decrease in the ejection fraction and fractional shortening at 2 and

4 weeks as compared to 1 week. In the IONP-NV + M group, cardiac contractibility, such as ejection fraction and fractional shortening, was preserved or increased during the 4-week follow-up period (Fig. 6, E and F). In addition, there was no significant difference in the left ventricular end diastolic dimension (LVIDd) among all groups except for the normal group (Fig. 6G). However, the left ventricular end systolic dimension (LVIDs) was significantly lower in the IONP-NV + M group than in the NT group and the IONP group at 4 weeks (Fig. 6H). Furthermore, there was no significant difference in the posterior wall thickness among all groups (Fig. 6I). However, septal wall thickness was significantly higher in the IONP-NV + M group than in other groups at 4 weeks (Fig. 6J). In
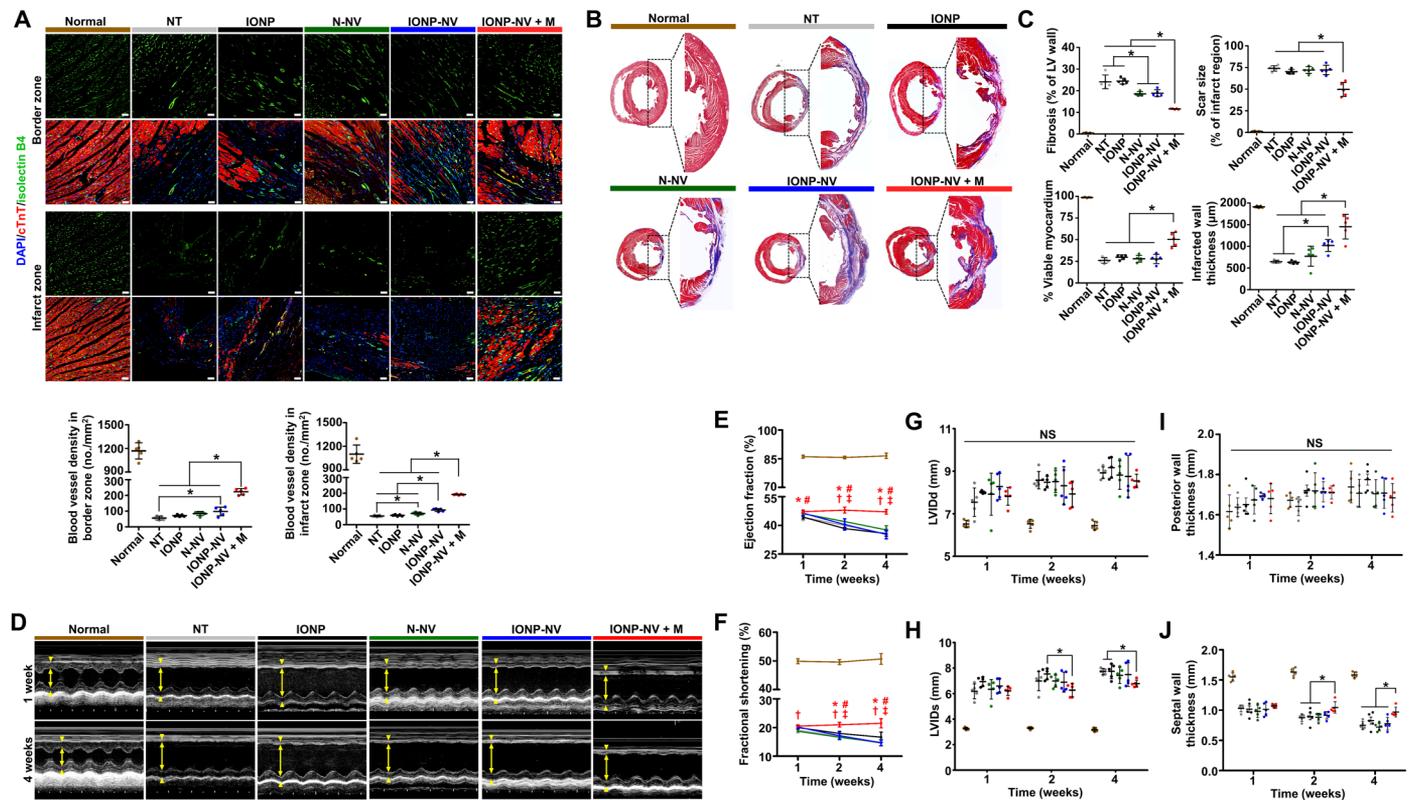
Fig. 6. Enhanced blood vessel density, the improvement of left ventricular remodeling, and the promotion of cardiac function recovery. (**A**) Representative images of functional blood vessels visualized by perfusion of isolectin B4 and immunostaining for cTnT (CM marker) in the infarct zone and border zone 4 weeks after injection and the quantitative data (*n* = 5 animals per group). Scale bars, 50 μm. (**B**) Representative Masson's trichrome–stained infarcted hearts four weeks after injection (blue, scar tissue; red, viable myocardium). (**C**) The fibrosis area, scar size, viable myocardium area, and thickness of the left ventricular (LV) wall 4 weeks after injection (*n* = 5 animals per group). *$P < 0.05$, using one-way ANOVA, followed by post hoc Bonferroni test. (**D**) Representative M-mode images 1 and 4 weeks after treatment. Yellow arrows between wall motions indicate left ventricular dimension. Distance between yellow arrows and arrowheads in top and bottom area indicates left ventricular wall thickness and left ventricular posterior wall thickness, respectively. (**E** and **F**) Ejection fraction and fractional shortening at various time points (*n* = 5 animals per group). *$P < 0.05$ versus NT, #$P < 0.05$ versus IONP, †$P < 0.05$ versus N-NV, and ‡$P < 0.05$ versus IONP-NV, using two-way ANOVA, followed by post hoc Bonferroni test. (**G** and **H**) Left ventricular end diastolic dimension (LVIDd) and left ventricular end systolic dimension (LVIDs) at various time points (*n* = 5 animals per group). (**I** and **J**) Posterior wall thickness and septal wall thickness at various time points (*n* = 5 animals per group). *$P < 0.05$, using two-way ANOVA, followed by post hoc Bonferroni test. The group names in (E to J) are referred to Fig. 6 (C and D). All values are means ± SD.

addition, we further assessed dose-dependent therapeutic effects of IONP-NVs with magnetic guidance (fig. S10, A and B). IONP-NVs improved the cardiac functions dose dependently in 1.0× and 3.0× compared to NT group but not in 0.3×. The heart functions were not different between 1.0× IONP-NVs and 3.0× IONP-NVs. These data indicate that IONP-NVs with magnetic guidance can prevent adverse left ventricular remodeling and lead to cardiac function preservation, which is likely attributed to the high retention of injected IONP-NVs; attenuation of cell apoptosis, inflammation, and fibrosis; and the enhancement in blood vessel density in the infarcted myocardium (Figs. 5 and 6).

DISCUSSION

In this study, we developed therapeutic efficacy–potentiated and cardiac retention–enhanced IONP-NVs from IONP-MSCs for a cell-free therapy for MI. Our data indicate that (i) biodegradable IONPs increased the levels of cardiac repair–favorable molecules in MSCs without cytotoxicity (Fig. 1); (ii) IONP-NVs derived from

IONP-MSCs contained higher levels of therapeutic molecules than N-NVs derived from MSCs (Fig. 2); (iii) IONP-NVs were efficiently internalized into individual cell levels (CFs, CMs, ECs, and macrophages) and exhibited therapeutic efficacy on damaged cells in vitro, which was similar to the therapeutic effects of MSCs, showing the possibility of a cell-free therapy for MI (Fig. 3); (iv) in a rat MI model, magnetic guidance enhanced the retention of injected IONP-NVs within the MI injury site (Fig. 4); and (v) IONP-NV injection in the infracted heart under magnetic guidance facilitated cardiac repair via antiapoptosis, anti-inflammation, angiogenesis, and antifibrosis (Figs. 5 and 6).

We focused on the mechanisms of IONP-NVs for cardiac repair as antiapoptosis, antifibrosis, anti-inflammation, and proangiogenesis, which are known as the mechanisms of MSC-based cardiac repair. We confirmed that IONP up-regulated the therapeutic molecules, including ANG1, FGF2, HGF, VEGF, and Cx43 in IONP-MSCs and these up-regulated molecules were also retained in IONP-NVs. Mechanistically, IONPs not only induced up-regulation of HIF1α-mediated growth factor expression but also activated JNK and c-Jun,

which might up-regulate the expression of Cx43 in MSCs. We further verified that miRNAs associated with cardiac repair were relatively higher in IONP-NVs than those of N-NVs. However, the exact mechanisms of the up-regulation of miRNAs in IONP-NVs are still unknown, and additional studies will be needed to address these issues. miRNAs described in Fig. 2E, which were more retained in IONP-NVs than N-NVs, are already known to be involved in antiapoptosis, anti-inflammation, antifibrosis, proangiogenesis, and prevention of hypertrophy in infarcted heart by MSCs (41).

After MI, CFs are known to differentiate into cardiac myofibroblasts, which can exacerbate cardiac remodeling and lead to heart failure. Myofibroblasts produce extracellular matrix (ECM) and express high levels of *Tgfb1*, *Acta2*, and *Mmps* and a low level of *Timps* in infarcted heart, which leads to dynamic changes in ECM composition and the subsequent dilation of the heart (42). We demonstrate that IONP-NVs have antifibrotic effects by down-regulation of myofibroblast-specific gene expressions including *Acta2*, *Tgfb1*, and the ratio of *Mmps* to *Timps* (Fig. 3B). IONP-NVs may contribute to the prevention of ventricular remodeling by inhibiting the differentiation of CFs into cardiac myofibroblasts and controlling the balance between MMPs and TIMPs.

Previous studies have shown that most of the cells and exosomes therapy have low retention rates after intramyocardial injection, which may lead unsatisfactory therapeutic effect on cardiac repair (43, 44). NVs cannot function unless cardiac cells uptake them. Cells uptake NVs within 24 hours after NV injection (fig. S4, A and B). Thus, it would be important to retain injected NVs in the infarcted myocardium for at least 24 hours after injection. We demonstrated that magnetic guidance could significantly increase the retention of IONP-NVs in the infarcted myocardium at 24 hours (Fig. 4). The higher retention of NVs than that of MSCs may be due to the difference in the fate of NVs and MSCs following injection into infarcted myocardium. Most of the injected MSCs back-leak out from the injection site immediately after injection, and the remaining MSCs gradually die due to anoikis. Many injected NVs, however, are internalized into cardiac cells in infarcted heart, allowing them no opportunity to diffuse out.

Several previous studies have modified cells and exosomes with IONPs. Cheng *et al.* (43) showed that IONP-labeled cardiosphere-derived cells and magnetic guidance elicited increased retention of the cells in the heart. Hood *et al.* (45) isolated exosomes using IONPs but did not use the exosome for therapy. Hu *et al.* (46) and Busato *et al.* (39) used IONP-labeled exosomes for MRI. Qi *et al.* (47) modified exosomes with IONPs to increase exosome targeting to tumor and did not enhance the quantity of therapeutic molecules in the exosomes. However, in the present study, we developed MSC-derived IONP-NVs through a simple modification with IONPs, which have larger quantities of therapeutic molecules and a higher targeting efficiency than conventional MSC-derived NVs. We applied IONP-NVs in MI model and demonstrated higher therapeutic effects on cardiac repair than conventional MSC implantation therapy, which have not been demonstrated by the previous studies.

In summary, we demonstrate that therapeutic molecule–enriched and cardiac retention–enhanced IONP-NVs can improve the cardiac repair potency of NVs derived from MSCs. IONPs are biodegradable, nontoxic, and a U.S. Food and Drug Administration–approved material and are assimilated in the body. IONP-NVs may be an effective cell-free therapy that can replace MSC therapy for MI.

MATERIALS AND METHODS
Preparation of IONPs
IONPs were synthesized by a previously reported method (48). Two millimoles of iron (III) acetylacetonate, 4 mmol of oleic acid, 0.4 g of 4-biphenylcarboxylic acid, and 10 ml of benzyl ether were mixed in a three-neck round-bottomed flask. After degassing, the mixture solution was heated to 290°C at a heating rate of 20°C/min with vigorous stirring and aged for 30 min. The resulting product was cooled down to room temperature and washed with ethanol several times. As-synthesized IONPs were dispersed in chloroform to be transferred to water. Three milliliters of oleic acid–capped IONPs in chloroform (10 mg/ml) was mixed with 60 mg of 1,2-distearoyl-*sn*-glycero-3-phosphoethanolamine-*N*-[methoxy(polyethylene glycol)-2000] (DSPE-PEG2000; Avanti Polar Lipids Inc., Birmingham, AL, USA). The resulting mixture was vigorously sonicated for 5 min, and the solvent was evaporated using a rotary evaporator and vacuum oven. After 3 hours, distilled water was added, and the mixture was vigorously sonicated to disperse the nanoparticles. The final product was obtained after washing with distilled water and ultracentrifugation several times. To synthesize RITC-labeled IONPs, IONPs were transferred to water with a mixture of amine-functionalized DSPE-PEG2000 and DSPE-PEG2000 (1:10). RITC dissolved in dimethylformamide was added to the amine-functionalized IONPs. The mixture was shaken for 3 hours, and excessive RITC was removed using PD-10 column chromatography (GE Healthcare, Little Chalfont, UK). The final product was dissolved in distilled water. The concentration and the shape of IONPs were evaluated using ICP-MS (NexION 350D, PerkinElmer, Waltham, MA, USA), installed at the National Center for Inter-University Research Facilities at Seoul National University and TEM (JEM-1010, JEOL Ltd., Tokyo, Japan), respectively.

Cell culture
Human bone marrow MSCs were purchased from Lonza (Walkersville, MD, USA) and cultured according to the manufacturer's instructions. MSCs were cultured in Dulbecco's modified Eagle's medium high glucose (Gibco BRL, Gaithersburg, MD, USA) supplemented with 10% (v/v) fetal bovine serum (Gibco BRL) and 1% (v/v) penicillin/streptomycin (Gibco BRL). MSCs at passage under six were used for the experiments. For osteogenic differentiation of MSCs, we used an osteogenic induction medium containing Dulbecco's modified Eagle's medium high glucose with 10% (v/v) fetal bovine serum, 1% (v/v) penicillin/streptomycin, 100 nM dexamethasone (Sigma-Aldrich), ascorbate-2-phosphate (50 mg/liter; Sigma-Aldrich), and 10 mM β-glycerol phosphate (Sigma-Aldrich). For adipogenic differentiation of MSCs, we used an adipogenic induction medium containing Dulbecco's modified Eagle's medium high glucose with 10% (v/v) fetal bovine serum, 1% (v/v) penicillin/streptomycin, 500 μM 1-methyl-3-isobutylxanthine (Sigma-Aldrich), 1 μM dexamethasone, 200 μM indomethacin (Sigma-Aldrich), and insulin (10 μg/ml; Gibco BRL). For chondrogenic differentiation of MSCs, we used a chondrogenic induction medium containing Dulbecco's modified Eagle's medium high glucose with 1% (v/v) penicillin/streptomycin and transforming growth factor β3 (10 ng/ml) after forming pellets. For the preparation of IONP-MSC, IONPs were added to a MSC culture at a concentration of 40 μg/ml. One day after the IONP treatment, IONP-treated MSCs were washed with phosphate-buffered saline (PBS; Gibco BRL) three times for the thorough removal of IONPs retained in the culture medium. The cells were cultured for 24 hours in fresh medium and then analyzed or collected to produce

NVs or for the use in vitro and in vivo experiments. Rat CMs were purchased from Lonza and cultured in Rat Cardiac Growth Medium (Lonza) on fibronectin-coated culture plates. Rat CFs were purchased from ScienCell (San Diego, CA, USA) and cultured in Fibroblast Medium-2 (ScienCell) on poly-L-lysine–coated culture plates. HUVECs were purchased from Lonza and cultured in Endothelial Cell Growth Medium-2 (Lonza) on tissue culture plates. HUVECs at a passage under seven were used for the experiments. RAW 264.7 cell line was purchased from Korean Cell Line Bank (Seoul, South Korea) and cultured in Dulbecco's modified Eagle medium high glucose supplemented with 10% (v/v) fetal bovine serum (Gibco BRL) and 1% (v/v) penicillin/streptomycin on tissue culture plates.

Preparation of NVs
NVs were prepared from MSCs and IONP-MSCs using a modification of a previously described method (19). The cells were detached using a cell scraper. The cells were suspended in PBS concentration of at least 1×10^6 cells/ml or placed in −80°C before the extrusion. The cells were extruded five to six times through 10- and 5-μm and 400-nm pore-sized polycarbonate membrane filters (Whatman Inc., Clifton, NJ, USA) with a mini extruder (Avanti Polar Lipids). To separate NVs from free proteins and cellular debris, a gradient solution composed of iodixanol (Axis-Shield PoC AS, Oslo, Norway) was used. One milliliters of 50% iodixanol, 2 ml of 10% iodixanol, and 7 ml of the extruded samples were placed sequentially onto the bottom of an ultracentrifuge tube, and the tube was ultracentrifuged at 100,000g for 2 hours at 4°C. The fraction 3 and 4 (free IONPs, 1 ml) and the fraction 1 (free proteins and RNAs, 6.5 ml) of the tube were discarded after ultracentrifugation (fig. 3A). The fraction 2 (NV, 2.5 ml) of the ultracentrifuge tube was collected, and an additional ultracentrifugation was performed at 100,000g for 2 hours at 4°C. The pellet in the tube was resuspended in PBS and filtered with 0.45-μm syringe filter. In case of IONP-NVs, IONP-NVs (fraction 6) were further isolated from a mixture of N-NVs and IONP-NVs using magnet. The quantity of proteins of each fraction was determined using Bradford assay as previously described (20). The quantity of IONPs of each fractions was measured using ICP-MS. Approximately, 100 to 150 μg of NVs were produced from 1×10^6 cells. IONP-NVs and N-NVs were stored at −80°C before use.

Characterization of IONP-MSCs and IONP-NVs
The plasma membranes of MSCs and NVs were labeled with 3,3′-dioctadecyloxacarbocyanine perchlorate (DiO). IONPs were labeled with RITC. IONP-MSCs were fixed with 4% paraformaldehyde (PFA) for 10 min and mounted with a mounting solution containing 4′,6-diamidino-2-phenylindole (DAPI) (Vector Laboratories Inc., Burlingame, CA, USA) that stains the nuclei. The samples were photographed using a fluorescence microscope (Olympus, Tokyo, Japan). For the TEM analysis, IONP-MSCs were fixed using Karnovsky's fixative solution for 2 hours at 4°C, washed three times with 0.05 M sodium cacodylate buffer, fixed with 1% osmium tetraoxide for 2 hours at 4°C, and rinsed twice with distilled water. The samples were stained using 0.5% uranyl acetate overnight at 4°C, dehydrated with an ethanol series (30, 50, 70, 80, 90, and 100%), infiltrated with propylene oxide, embedded in Spurr's resin, and cut into thin sections with a thickness of 100 nm using an ultramicrotome (Leica, Wetzlar, Germany). The thin sections of IONP-MSCs, uranyl acetate–labeled N-NVs, and IONP-NVs were collected onto 200-mesh copper grids and imaged using a TEM. To further confirm the presence of IONPs

in IONP-NVs, STEM and EDX mapping were performed. To evaluate the contents of IONPs within MSCs, IONP-MSCs were analyzed using ICP-MS. To assess the internalization of IONPs into NVs, image acquisition was performed using super-resolution microscope (Elyra PS. 1, Carl Zeiss, Oberkochen, Germany). The size distribution of NVs was determined using a DLS (DLS-7000, Otsuka Electronics, Osaka, Japan). To determine in vitro cellular uptake rate of NVs, 10 μg of IONP-NVs (200 ng of Fe) were treated to macrophages after the treatment with mitomycin C (10 μg/ml; Sigma-Aldrich, St. Louis, MO, USA) for 2 hours for the inhibition of cell proliferation. At 0, 6, 12, 24, and 48 hours, iron content in macrophages were analyzed using ICP-MS. To determine intracellular iron content in the cells after the IONP-NV treatment, CMs, CFs, HUVECs, and macrophages were treated with mitomycin C for the inhibition of cell proliferation for 2 hours and subsequently treated with IONP-NVs (20 μg/ml) for 24 hours. Then, the medium was changed with fresh medium. The iron content in the CMs, CFs, HUVECs, and macrophages was analyzed using ICP-MS 1, 5, 10, and 14 days after the IONP-NV treatment.

qPCR and analysis of RNA
RNA quantity and expression were evaluated using qRT-PCR. Cell, NV ($n = 4$), and tissue samples ($n = 5$) were lysed using 1 ml of the TRIzol reagent (Invitrogen, Carlsbad, CA, USA), and total RNA was extracted using 200 μl of chloroform. The samples were centrifuged at 10,000g for 10 min at 4°C. The supernatant was collected, mixed with 80% (v/v) isopropanol in water, and centrifuged at 10,000g for 10 min at 4°C. The RNA pellet was rinsed with 75% (v/v) ethanol, dried, and dissolved in ribonuclease-free water. Complementary DNA was reverse-transcribed from RNA using the AccuPower RT PreMix (Bioneer, Daejeon, South Korea). Gene expressions were evaluated using the StepOnePlus Real-Time PCR System (Applied Biosystems, Foster City, CA, USA). Glyceraldehyde 3-phosphate dehydrogenase served as the housekeeping genes. The primer sequences for the qRT-PCR are described in tables S1 to S3. Expressions of miRNA and mRNA were analyzed using Affymetrix 4.0 microarray (Thermo Fisher Scientific) and NovaSeq (Illumina, CA, USA), respectively. A total of 343 miRNAs and 227 mRNAs were identified to be differentially included in IONP-NVs versus N-NVs.

Evaluation of cellular viability
Cell viability was determined using the CCK assay and FDA/EB staining. For the CCK assay, 50 μl of EZ-CYTOX per well (Daeil Lab Service, Changwon, South Korea) was added to 24-well culture plates and incubated for 2 hours at 37°C. The absorbance of the solution was measured at 450 nm using a spectrophotometer. For the FDA/EB staining, 1 ml of FDA (5 μg/ml; Sigma-Aldrich) and EB (10 μg/ml; Sigma-Aldrich) solution was added to each well of six-well culture plates and incubated 5 min at 37°C. Staining was then photographed with a fluorescence microscope (Olympus). The viability of MSCs and IONP-MSCs was quantified using the CCK assay 2, 4, 7, 10, and 14 days after the IONP treatment and was qualified with the FDA/EB staining 2 days after the IONP treatment. To compare the cytotoxicity of direct treatment of iron ions, MSCs were treated with the same molar concentration of $Fe^{2+/3+}$ as that of IONPs (40 μg/ml). The viability of the CFs, CMs, and HUVECs was quantified with the CCK assay and the FDA/EB staining 1 day after coculture and NV treatment. For the evaluation of the cytotoxicity of IONPs and IONP-NVs, the viability of the CFs, CMs, and HUVECs was quantified with the CCK assay 2, 5, and 10 days after treatment.

At least three samples per group were used for the 3-(4,5-dimethylthiazol-2-yl)-2,5-diphenyltetrazolium bromide (MTT) assay, CCK assay, and FDA/EB staining.

Western blot analysis

Western blot analysis was used to evaluate the protein expression or quantity within the cell, NV, and tissue samples ($n = 3$). Cell or NV or tissue samples were lysed by SDS sample buffer [62.5 mM tris-HCl (pH 6.8), 2% (w/v) SDS, 10% (v/v) glycerol, 50 mM dithiothreitol, and 0.1% (w/v) bromophenol blue]. Proteins were separated by 10% SDS–polyacrylamide gel electrophoresis and transferred to an Immobilon-P membrane (Millipore Corp., Bedford, MA, USA). For specific protein detection, primary antibodies against β-actin, ANG1, FGF2, VEGF, HGF, HIF1α, Cx43, ERK1/2, pERK1/2, PCNA, and CD9 (these antibodies were purchased from Abcam, Cambridge, UK) as well as against c-Jun, pc-Jun, JNK, pJNK, AKT, pAKT, and PI3K (these antibodies were purchased from Cell Signaling Technology, MA, USA) were incubated with membranes overnight at 4°C. The membranes were washed three times and incubated with secondary antibodies conjugated with horseradish peroxidase (Sigma-Aldrich) for 1 hour at room temperature. The blots were developed using chemiluminescence (LumiGLO, KPL Europe, Guildford, UK). Quantification of the Western blots was evaluated using the ImageJ software.

Characterization of NVs and exosomes

IONP-MSC–derived exosomes were isolated by serial centrifugation of IONP-MSC–conditioned medium. To assess the number of particles of NVs and exosomes, nanoparticle tracking analysis was used. To assess the protein quantity, NVs and exosomes were lysed, and then the protein quantity was determined using bicinchoninic acid assay. To assess the RNA quantity, NVs and exosomes were lysed using TRIzol, and then the RNA quantity was determined using NanoDrop (Thermo Fisher Scientific, MA, USA).

In vitro cell assay under hypoxic conditions and macrophage polarization by the NV treatment

To generate hypoxic culture conditions for the CFs, CMs, and HUVECs, the cell culture was carried out in a hypoxic incubator (MCO-18M, Sanyo, Japan) containing 1% O_2 for 6 hours at 37°C. To polarize macrophages into M1 phenotype, RAW 264.7 cell line was cultured in the presence of lipopolysaccharide (LPS) (100 ng/ml; Sigma-Aldrich) for 1 day. After establishing the hypoxic culture or M1 polarization, the cells were cocultured with MSCs or IONP-MSCs or were treated with IONP (420 ng/ml), N-NVs, or IONP-NVs (20 μg/ml) for 24 hours. Then, the medium was changed with fresh medium. Cells were cultured for 1 day and used for the analysis. To control the equal dose of NVs and the number of MSCs for coculture, the yield of NVs from MSCs was applied. One hundred fifty micrograms of NVs were treated against 1×10^6 cocultured MSCs.

Capillary tube formation

Cell culture plates were coated with Geltrex (Invitrogen) and incubated for 30 min at 37°C to promote gelation. HUVECs underwent hypoxic condition (1% O_2) and were simultaneously cocultured with MSCs or IONP-MSCs (1.5×10^5 cells) using transwells (Corning, New York, USA) or treated with IONP (420 ng/ml), N-NVs, or IONP-NVs (20 μg/ml) for 6 hours and be subsequently detached using trypsin. Then, HUVECs were plated at 5×10^4 cells/cm^2 on the Geltrex for 6 hours at 37°C. Capillary tubes were observed using

a light microscope. Six random fields were measured for the quantitative analysis.

Cell migration assay

HUVECs were seeded on culture plates, grown until confluence. HUVECs underwent hypoxic condition (1% O_2) and were simultaneously cocultured with MSCs or IONP-MSCs (1.5×10^5 cells) using transwells (Corning, New York, USA) or treated with IONP (420 ng/ml), N-NVs, or IONP-NVs (20 μg/ml) for 6 hours and then incubated under hypoxic conditions (1% O_2) for 6 hours at 37°C. Next, a linear gap was created by scratching the surface of the culture plates using a sterile yellow tip. The cells were rinsed three times with PBS to thoroughly remove the detached cells. After 12 hours, five random fields were photographed and quantified using the following equation: [(initial cell-free area − cell-free area at 12 hours)/initial cell-free area] × 100%. Quantification of the scratched area was evaluated using the ImageJ software.

MI and treatment

The animal studies were approved by The Catholic University of Korea Animal Care and Use Committee and Institutional Animal Care and Use Committee and Department of Laboratory Animal in The Catholic University of Korea, Songeui Campus accredited the Korea Excellence Animal Laboratory Facility from Korea Food and Drug Administration in 2017 and acquired Association for Assessment and Accreditation of Laboratory Animal Care International full accreditation in 2018 (CUMC-2017-0240-04). Fischer 344 rats (180 to 200 g, 8-week-old male; KOATECH, Korea) were anesthetized with 2% inhaled isoflurane and intubated via the trachea with an 18-gauge intravenous catheter. The rats were then mechanically ventilated with medical grade oxygen. Animals were placed on a 37°C heating pad to prevent cooling during the procedure. After shaving the chest, a left thoracotomy was performed. MI was achieved by tying a suture with a sterile polyethylene glycol tubing (22 gauges) that was placed into the left anterior descending artery for 1 min, and then the knot was permanently ligated using 7-0 Prolene suture. One day after the ligation, the rats were anesthetized again using isoflurane inhalation and intubated and mechanically ventilated. The animal chest was reopened, and IONP (3.15 μg), IONP-MSC (1×10^6 cells), MSC (1×10^6 cells), N-NV (150 μg), or IONP-NV (150 μg) in 100 μl of PBS was injected at four different sites in the border zone of the infarcted myocardium. For the IONP-NV + M group, a neodymium magnet (diameter, 15 mm; thickness, 5 mm) was immobilized on the heart for 5 min just after injection. After closing the chest, the magnet was implanted into the muscle above the heart and removed after 24 hours.

Magnetic resonance imaging

Endotracheal intubation was performed with 18-gauge angiocatheter. The rats were anesthetized with inhaled 2% isoflurane and then mechanically ventilated with medical grade oxygen. Subsequently, 0.9% NaCl solution was perfused for 5 min into the right internal jugular vein using a perfusion pump. As the perfusion with 0.9% NaCl solution started, descending thoracic aorta and inferior vena cava were incised to rapidly clear the blood from the animals. Afterward, 0.9% NaCl solution was changed to 10% MultiHance (Bracco, Italy) in 4% PFA solution for perfusion for 10 min to fix the heart tissues. The hearts were harvested when the perfusion process was completed. To retain the shape of the harvested tissue, 1.5% agarose

solution was perfused into the aorta until the agarose solution was visible from the incised heart region and aorta. MRI was performed with a 9.4T MRI system with a 70-mm active decoupling quad volume coil (Agilent Technologies, Santa Clara, CA, USA). Conditions for spin-echo T2-weighted imaging are as follows: repetition time, 3000 ms; echo time, 10 ms; number of excitations, 5; matrix, 256 by 256; slice thickness, 0.5 mm; field of view, 35 mm by 35 mm; scan time, 21 min and 36 s. For T_2 relaxation time measurements, the Carr-Purcell-Meiboon-Gill pulse sequence was adapted for multiple spin echo measurements. Thirty-four images were acquired with 34 different echo time values ranging from 8 to 160 ms. T_2 relaxation times were obtained from the nonlinear least squares fit of the mean pixel values for the multiple spin echo measurements at each echo time. Relaxivities (R_2) were then calculated as an inverse of relaxation time per millimolar.

Assessment of NV retention in the infarcted myocardium

For quantitative evaluation of the retention of cells and NVs in the infarcted myocardium, the plasma membranes of the cells and NVs were labeled with VivoTrack 680 (PerkinElmer) for 2 hours before intramyocardial injection. We intramyocardially injected 1×10^6 MSCs and IONP-MSCs or 150 μg of N-NVs and IONP-NVs, and magnetic guidance was applied for 24 hours or not. To confirm the dose-dependent therapeutic effects of IONP-NVs, we injected 0.3×, 1.0×, and 3.0× (1.0× = 150 μg of IONP-NVs per animal) into infarcted hearts. At the time points of 6, 24, and 48 hours after injection, the animals were euthanized, and the fluorescence intensity was measured with harvested hearts and other organs using an eXplore Optix system (Advanced Research Technologies Inc., Montreal, Canada). The initial fluorescence intensity of the cells and NVs was evaluated. The retention ratio was calculated by the following equation: (fluorescence intensity in the heart at 24 hours/initial fluorescence intensity of IONP-MSCs or IONP-NVs) × 100%. To further visualize the retention of NVs in the infarcted myocardium, the plasma membranes of NVs were labeled with 1,1′-dioctadecyl-3,3,3′,3′-tetramethylindocarbocyanine perchlorate for 2 hours and injected into the myocardium. After the animals were euthanized, the heart tissues were fixed with formaldehyde for 24 hours, embedded in paraffin, and sliced into a 4-μm thickness. The tissue sections were photographed using a fluorescent microscope (Olympus) after reducing background fluorescent signals with Dako Antibody Diluent Background Reducing Components (Agilent Technologies). For the detection of IONPs, Prussian blue staining was performed in major organs including the lung, heart, kidney, liver, and spleen 1 and 4 weeks after the injection of IONP-NVs. Magnetic guidance was applied for 1 day. Nuclear fast red staining was used for counterstaining.

In vivo apoptosis, inflammation, and toxicity after treatment

To evaluate the antiapoptotic and anti-inflammatory effects of N-NVs and IONP-NVs, the heart tissues were obtained 1 day after injection. For the apoptotic cell evaluation, tissue sections were analyzed using the TUNEL assay and quantified. To compare gene expression patterns in the infarcted myocardium, the MI region of the heart was analyzed by qRT-PCR for M2 macrophage markers (*Cd206*, *Arg1*, and *Il10*) and M1 macrophage markers (*Nos2*, *Il1b*, and *Il6*). For toxicity analysis, serum from the whole blood was collected at the various time points. The levels of ALT, AST, BUN, and creatinine were evaluated using a chemistry analyzer (DRI-CHEM 3500s, Fujifilm, Tokyo, Japan).

Immunohistochemical assessment after treatment

For immunohistochemical analysis of M1 and M2 macrophages and Cx43, the heart tissues were obtained 1 day after treatment. Tissue sections were treated with proteinase K for 15 min at 37°C. The nonspecific region was blocked with normal goat serum (Sigma-Aldrich). Then, the slides were incubated with primary antibodies against cardiac troponin T (cTnT), Cx43, CD68, CD206, and NOS2 (these antibodies were purchased from Abcam), diluted with Dako Antibody Diluent Background Reducing Components (Agilent Technologies) at 4°C overnight. The slides were washed three times with PBS, incubated for 1 hour with rhodamine-conjugated secondary antibodies at room temperature, washed, mounted with a mounting medium (Vector Laboratories Inc.), and photographed using fluorescent microscope (Olympus).

Capillary density determination

At the time of euthanasia, the hearts were perfused with green fluorescent protein–conjugated isolectin B4 from Griffonia simplicifolia for 15 min at room temperature. Then, the hearts were fixed in 4% PFA overnight, embedded in paraffin, and sectioned in 4-μm-thick slices. The number of blood vessels was counted in five random microscopic fields using a fluorescence microscope.

Determination of fibrosis

Masson's trichrome (Sigma-Aldrich) staining was performed to determine the fibrosis area of the MI hearts. Briefly, three tissue sections in each group were fixed in Bouin's solution at 56°C for 1 hour, stained using Weigert's iron hematoxylin solution for 15 min at room temperature, and stained using Biebrich scarlet-acid fuchsin solution for 10 min at room temperature. Last, the sections were counterstained with aniline blue for 15 min, followed by incubation in 0.2% acetic acid for 1 min at room temperature. The collagen fibers appear as blue, and viable myocardium appears as red. The area of fibrosis to the entire left ventricular wall area was quantified with the ImageJ software.

Evaluation of cardiac functions

The assessment of cardiac functions was performed with echocardiography. The rats were lightly anesthetized with inhaled 2% isoflurane, and physiological data were recorded with a transthoracic echocardiography system equipped with a 15-MHz L15-7io linear transducer (Affiniti 50G, Philips). Different echocardiograms were performed at 1, 2, and 4 weeks after MI. The echocardiography operator was blinded to the group allocation during the experiment. Ejection fraction and fractional shortening, which are indexes of the left ventricular systolic function, were calculated using a previously described method (*49*).

Statistical analysis

All quantitative data are expressed as the means ± SD. Two-tailed Student's *t* test was used for comparison between two groups. A one-way and two-way analysis of variance (ANOVA) followed by Bonferroni test was used for all statistical analysis. A difference with a $P < 0.05$ was considered statistically significant. All statistical analyses were performed using Prism 7.0 (GraphPad Software Inc.).

REFERENCES AND NOTES

1. T. A. Gaziano, Cardiovascular disease in the developing world and its cost-effective management. *Circulation* **112**, 3547–3553 (2005).

2. Writing Group Members, D. Mozaffarian, E. J. Benjamin, A. S. Go, D. K. Arnett, M. J. Blaha, M. Cushman, S. R. Das, S. de Ferranti, J. P. Després, H. J. Fullerton, V. J. Howard, M. D. Huffman, C. R. Isasi, M. C. Jiménez, S. E. Judd, B. M. Kissela, J. H. Lichtman, L. D. Lisabeth, S. Liu, R. H. Mackey, D. J. Magid, D. K. McGuire, E. R. Mohler III, C. S. Moy, P. Muntner, M. E. Mussolino, K. Nasir, R. W. Neumar, L. Palaniappan, D. K. Pandey, M. J. Reeves, C. J. Rodriguez, W. Rosamond, P. D. Sorlie, J. Stein, A. Towfighi, T. N. Turan, S. S. Virani, D. Woo, R. W. Yeh; American Heart Association Statistics Committee; Stroke Statistics Subcommittee, Heart disease and stroke statistics-2016 update: A report from the american heart association. *Circulation* **133**, E38–E360 (2016).

3. L. C. Amado, A. P. Saliaris, K. H. Schuleri, M. St John, J. S. Xie, S. Cattaneo, D. J. Durand, T. Fitton, J. Q. Kuang, G. Stewart, S. Lehrke, W. W. Baumgartner, B. J. Martin, A. W. Heldman, J. M. Hare, Cardiac repair with intramyocardial injection of allogeneic mesenchymal stem cells after myocardial infarction. *Proc. Natl. Acad. Sci. U.S.A.* **102**, 11474–11479 (2005).

4. J. G. Shake, P. J. Gruber, W. A. Baumgartner, G. Senechal, J. Meyers, J. M. Redmond, M. F. Pittenger, B. J. Martin, Mesenchymal stem cell implantation in a swine myocardial infarct model: Engraftment and functional effects. *Ann. Thorac. Surg.* **73**, 1919–1925 (2002).

5. R. Delewi, A. Andriessen, J. G. P. Tijssen, F. Zijlstra, J. J. Piek, A. Hirsch, Impact of intracoronary cell therapy on left ventricular function in the setting of acute myocardial infarction: A meta-analysis of randomised controlled clinical trials. *Heart* **99**, 225–232 (2013).

6. S. B. Seif-Naraghi, J. M. Singelyn, M. A. Salvatore, K. G. Osborn, J. J. Wang, U. Sampat, O. L. Kwan, G. M. Strachan, J. Wong, P. J. Schup-Magoffin, R. L. Braden, K. Bartels, J. A. DeQuach, M. Preul, A. M. Kinsey, A. N. DeMaria, N. Dib, K. L. Christman, Safety and efficacy of an injectable extracellular matrix hydrogel for treating myocardial infarction. *Sci. Transl. Med.* **5**, 173ra25 (2013).

7. S. L. Beeres, K. Zeppenfeld, J. J. Bax, E. E. Van der Wall, D. E. Atsma, M. J. Schalij, Electrophysiological and arrhythmogenic effects of intramyocardial bone marrow cell injection in patients with chronic ischemic heart disease. *Circulation* **114**, 606–606 (2006).

8. M. Breitbach, T. Bostani, W. Roell, Y. Xia, O. Dewald, J. M. Nygren, J. W. U. Fries, K. Tiemann, H. Bohlen, J. Hescheler, A. Welz, W. Bloch, S. E. W. Jacobsen, B. K. Fleischmann, Potential risks of bone marrow cell transplantation into infarcted hearts. *Blood* **110**, 1362–1369 (2007).

9. M. Gnecchi, H. M. He, O. D. Liang, L. G. Melo, F. Morello, H. Mu, N. Noiseux, L. N. Zhang, R. E. Pratt, J. S. Ingwall, V. J. Dzau, Paracrine action accounts for marked protection of ischemic heart by Akt-modified mesenchymal stem cells. *Nat. Med.* **11**, 367–368 (2005).

10. R. C. Lai, F. Arslan, M. M. Lee, N. S. K. Sze, A. Choo, T. S. Chen, M. Salto-Tellez, L. Timmers, C. N. Lee, R. M. El Oakley, G. Pasterkamp, D. P. V. de Kleijn, S. K. Lim, Exosome secreted by MSC reduces myocardial ischemia/reperfusion injury. *Stem Cell Res.* **4**, 214–222 (2010).

11. S. Y. Bian, L. P. Zhang, L. F. Duan, X. Wang, Y. Min, H. P. Yu, Extracellular vesicles derived from human bone marrow mesenchymal stem cells promote angiogenesis in a rat myocardial infarction model. *J. Mol. Med.* **92**, 387–397 (2014).

12. X. Teng, L. Chen, W. Chen, J. Yang, Z. Yang, Z. Shen, Mesenchymal stem cell-derived exosomes improve the microenvironment of infarcted myocardium contributing to angiogenesis and anti-inflammation. *Cell. Physiol. Biochem.* **37**, 2415–2424 (2015).

13. H. Valadi, K. Ekström, A. Bossios, M. Sjostrand, J. J. Lee, J. O. Lötvall, Exosome-mediated transfer of mRNAs and microRNAs is a novel mechanism of genetic exchange between cells. *Nat. Cell Biol.* **9**, 654–659 (2007).

14. C. Bang, T. Thum, Exosomes: New players in cell-cell communication. *Int. J. Biochem. Cell Biol.* **44**, 2060–2064 (2012).

15. S. Safari, F. Malekvandfard, S. Babashah, A. Alizadehasl, M. Sadeghizadeh, M. Motavaf, Mesenchymal stem cell-derived exosomes: A novel potential therapeutic avenue for cardiac regeneration. *Cell. Mol. Biol.* **62**, 66–73 (2016).

16. T. Katsuda, R. Tsuchiya, N. Kosaka, Y. Yoshioka, K. Takagaki, K. Oki, F. Takeshita, Y. Sakai, M. Kuroda, T. Ochiya, Human adipose tissue-derived mesenchymal stem cells secrete functional neprilysin-bound exosomes. *Sci. Rep.* **3**, 1197 (2013).

17. S. Dai, D. Wei, Z. Wu, X. Zhou, X. Wei, H. Huang, G. Li, Phase I clinical trial of autologous ascites-derived exosomes combined with GM-CSF for colorectal cancer. *Mol. Ther.* **16**, 782–790 (2008).

18. W. Jo, D. Jeong, J. Kim, J. Park, Self-renewal of bone marrow stem cells by nanovesicles engineered from embryonic stem cells. *Adv. Healthc. Mater.* **5**, 3148–3156 (2016).

19. K. Oh, S. R. Kim, D. K. Kim, M. W. Seo, C. Lee, H. M. Lee, J. E. Oh, E. Y. Choi, D. S. Lee, Y. S. Gho, K. S. Park, In vivo differentiation of therapeutic insulin-producing cells from bone marrow cells via extracellular vesicle-mimetic nanovesicles. *ACS Nano* **9**, 11718–11727 (2015).

20. W. Jo, J. Kim, J. Yoon, D. Jeong, S. Cho, H. Jeong, Y. J. Yoon, S. C. Kim, Y. S. Gho, J. Park, Large-scale generation of cell-derived nanovesicles. *Nanoscale* **6**, 12056–12064 (2014).

21. J. Kolosnjaj-Tabi, L. Lartigue, Y. Javed, N. Luciani, T. Pellegrino, C. Wilhelm, D. Alloyeau, F. Gazeau, Biotransformations of magnetic nanoparticles in the body. *Nano Today* **11**, 280–284 (2016).

22. M. I. Khan, A. Mohammad, G. Patil, S. A. H. Naqvi, L. K. S. Chauhan, I. Ahmad, Induction of ROS, mitochondrial damage and autophagy in lung epithelial cancer cells by iron oxide nanoparticles. *Biomaterials* **33**, 1477–1488 (2012).

23. Y. Y. C. Lo, J. M. S. Wong, T. F. Cruz, Reactive oxygen species mediate cytokine activation of c-jun NH2-terminal kinases. *J. Biol. Chem.* **271**, 15703–15707 (1996).

24. L. Li, Z. W. Feng, A. G. Porter, JNK-dependent phosphorylation of c-Jun on serine 63 mediates nitric oxide-induced apoptosis of neuroblastoma cells. *J. Biol. Chem.* **279**, 4058–4065 (2004).

25. S. Bonello, C. Zähringer, R. S. BelAiba, T. Djordjevic, J. Hess, C. Michiels, T. Kietzmann, A. Görlach, Reactive oxygen species activate the HIF-1α promoter via a functional NF kappa B site. *Arter. Thromb. Vasc. Biol.* **27**, 755–761 (2007).

26. K. Li, Y. Chi, K. Gao, Q. J. Yan, H. Matsue, M. Takeda, M. Kitamura, J. Yao, Connexin43 hemichannel-mediated regulation of connexin43. *PLOS ONE* **8**, e58057 (2013).

27. B. L. Krock, N. Skuli, M. C. Simon, Hypoxia-induced angiogenesis: Good and evil. *Genes Cancer* **2**, 1117–1133 (2011).

28. E. Minet, D. Mottet, G. Michel, I. Roland, M. Raes, J. Remacle, C. Michiels, Hypoxia-induced activation of HIF-1, role of HIF-1α-Hsp90 interaction. *FEBS Lett.* **460**, 251–256 (1999).

29. L. Kostura, D. L. Kraitchman, A. M. Mackay, M. F. Pittenger, J. W. M. Bulte, Feridex labeling of mesenchymal stem cells inhibits chondrogenesis but not adipogenesis or osteogenesis. *NMR Biomed.* **17**, 513–517 (2004).

30. N. Singh, G. J. Jenkins, R. Asadi, S. H. Doak, Potential toxicity of superparamagnetic iron oxide nanoparticles (SPION). *Nano Rev.* **1**, 5358 (2010).

31. M. J. Turk, J. A. Reddy, J. A. Chmielewski, P. S. Low, Characterization of a novel pH-sensitive peptide that enhances drug release from folate-targeted liposomes at endosomal pHs. *Biochim. Biophys. Acta* **1559**, 56–68 (2002).

32. L. Kordelas, V. Rebmann, A. K. Ludwig, S. Radtke, J. Ruesing, T. R. Doeppner, M. Epple, P. A. Horn, D. W. Beelen, B. Giebel, MSC-derived exosomes: A novel tool to treat therapy-refractory graft-versus-host disease. *Leukemia* **28**, 970–973 (2014).

33. J. Han, B. Kim, J. Y. Shin, S. Ryu, M. Noh, J. Woo, J. S. Park, Y. Lee, N. Lee, T. Hyeon, D. Choi, B. S. Kim, Iron oxide nanoparticle-mediated development of cellular gap junction crosstalk to improve mesenchymal stem cells' therapeutic efficacy for myocardial infarction. *ACS Nano* **9**, 2805–2819 (2015).

34. F. Arslan, R. C. Lai, M. B. Smeets, L. Akeroyd, A. Choo, E. N. E. Aguor, L. Timmers, H. V. van Rijen, P. A. Doevendans, G. Pasterkamp, S. K. Lim, D. P. de Kleijn, Mesenchymal stem cell-derived exosomes increase ATP levels, decrease oxidative stress and activate PI3K/Akt pathway to enhance myocardial viability and prevent adverse remodeling after myocardial ischemia/reperfusion injury. *Stem Cell Res.* **10**, 301–312 (2013).

35. N. Zeevi-Levin, Y. D. Barac, Y. Reisner, I. Reiter, G. Yaniv, G. Meiry, Z. Abassi, S. Kostin, J. Schaper, M. R. Rosen, N. Resnick, O. Binah, Gap junctional remodeling by hypoxia in cultured neonatal rat ventricular myocytes. *Cardiovasc. Res.* **66**, 64–73 (2005).

36. N. J. Severs, A. F. Bruce, E. Dupont, S. Rothery, Remodelling of gap junctions and connexin expression in diseased myocardium. *Cardiovasc. Res.* **80**, 9–19 (2008).

37. R. Eguchi, H. Naitou, K. Kunimasa, A. Ayuzawa, Y. Fujimori, N. Ohashi, K. Kaji, T. Ohta, Proteomic analysis of hypoxia-induced tube breakdown of an in vitro capillary model composed of HUVECs: Potential role of p38-regulated reduction of HSP27. *Proteomics* **8**, 2897–2906 (2008).

38. C. Toma, M. F. Pittenger, K. S. Cahill, B. J. Byrne, P. D. Kessler, Human mesenchymal stem cells differentiate to a cardiomyocyte phenotype in the adult murine heart. *Circulation* **105**, 93–98 (2002).

39. A. Busato, R. Bonafede, P. Bontempi, I. Scambi, L. Schiaffino, D. Benati, V. Malatesta, A. Sbarbati, P. Marzola, R. Mariotti, Magnetic resonance imaging of ultrasmall superparamagnetic iron oxide-labeled exosomes from stem cells: A new method to obtain labeled exosomes. *Int. J. Nanomedicine* **11**, 2481–2490 (2016).

40. J. Han, Y. S. Kim, M. Y. Lim, H. Y. Kim, S. Kong, M. Kang, Y. W. Choo, J. H. Jun, S. Ryu, H. Y. Jeong, J. Park, G. J. Jeong, J. C. Lee, G. H. Eom, Y. Ahn, B. S. Kim, Dual Roles of Graphene Oxide To attenuate inflammation and elicit timely polarization of macrophage phenotypes for cardiac repair. *ACS Nano* **12**, 1959–1977 (2018).

41. Z. Z. Wen, S. X. Zheng, C. Q. Zhou, W. L. Yuan, J. F. Wang, T. Wang, Bone marrow mesenchymal stem cells for post-myocardial infarction cardiac repair: MicroRNAs as novel regulators. *J. Cell. Mol. Med.* **16**, 657–671 (2012).

42. K. E. Porter, N. A. Turner, Cardiac fibroblasts: At the heart of myocardial remodeling. *Pharmacol. Ther.* **123**, 255–278 (2009).

43. K. Cheng, T. S. Li, K. Malliaras, D. R. Davis, Y. Q. Zhang, E. Marbán, Magnetic targeting enhances engraftment and functional benefit of iron-labeled cardiosphere-derived cells in myocardial infarction. *Circ. Res.* **106**, 1570–1581 (2010).

44. R. Gallet, J. Dawkins, J. Valle, E. Simsolo, G. de Couto, R. Middleton, E. Tseliou, D. Luthringer, M. Kreke, R. R. Smith, L. Marban, B. Ghaleh, E. Marbán, Exosomes secreted

by cardiosphere-derived cells reduce scarring, attenuate adverse remodelling, and improve function in acute and chronic porcine myocardial infarction. *Eur. Heart J.* **38**, 201–211 (2017).

45. J. L. Hood, M. J. Scott, S. A. Wickline, Maximizing exosome colloidal stability following electroporation. *Anal. Biochem.* **448**, 41–49 (2014).

46. L. Z. Hu, S. A. Wickline, J. L. Hood, Magnetic resonance imaging of melanoma exosomes in lymph nodes. *Magn. Reson. Med.* **74**, 266–271 (2015).

47. H. Z. Qi, C. Y. Liu, L. X. Long, Y. Ren, S. S. Zhang, X. D. Chang, X. M. Qian, H. H. Jia, J. Zhao, J. J. Sun, X. Hou, X. B. Yuan, C. S. Kang, Blood exosomes endowed with magnetic and targeting properties for cancer therapy. *ACS Nano* **10**, 3323–3333 (2016).

48. N. Lee, Y. Choi, Y. Lee, M. Park, W. K. Moon, S. H. Choi, T. Hyeon, Water-dispersible ferrimagnetic iron oxide nanocubes with extremely high r_2 relaxivity for highly sensitive in vivo MRI of tumors. *Nano Lett.* **12**, 3217–3131 (2012).

49. J. Jang, H. -J. Park, S. W. Kim, H. Kim, J. Y. Park, S. J. Na, H. J. Kim, M. N. Park, S. H. Choi, S. H. Park, S. W. Kim, S.-M. Kwon, P.-J. Kim, D.-W. Cho, 3D printed complex tissue construct using stem cell-laden decellularized extracellular matrix bioinks for cardiac repair. *Biomaterials* **112**, 264–274 (2017).

Citation: J.-R. Lee, B.-W. Park, J. Kim, Y. W. Choo, H. Y. Kim, J.-K. Yoon, H. Kim, J.-W. Hwang, M. Kang, S. P. Kwon, S. Y. Song, I. O. Ko, J.-A. Park, K. Ban, T. Hyeon, H.-J. Park, B.-S. Kim, Nanovesicles derived from iron oxide nanoparticles–incorporated mesenchymal stem cells for cardiac repair. *Sci. Adv.* **6**, eaaz0952 (2020).